Finite-element simulation of residual stresses induced by laser shock peening in TC4 samples structurally similar to a turbine blade

A. Kostina, M. Zhelnin, A. Vedernikova, M. Bartolomei
Institute of Continuous Media Mechanics of the Ural Branch of Russian Academy of Science (ICMM UB RAS), Russia
kostina@icmm.ru, http://orcid.org/0000-0002-5721-3301
zhelnin.m@icmm.ru, http://orcid.org/0000-0003-4498-450X
terekhina.a@icmm.ru, http://orcid.org/0000-0003-1069-7887
bartolomei.m@icmm.ru, http://orcid.org/0009-0003-3193-7605

S. Swaroop
Vellore Institute of Technology, India
n.r.sathya.swaroop@gmail.com, https://orcid.org/0000-0001-9872-811X

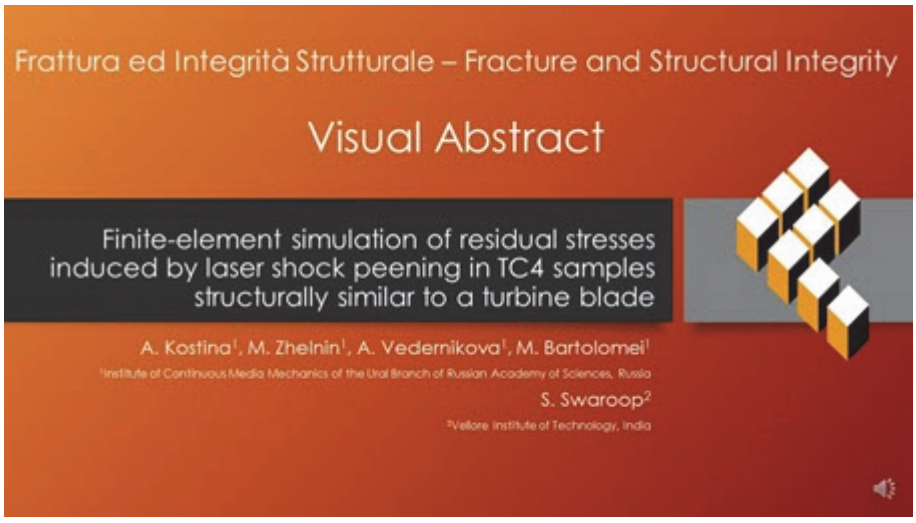

Citation: Kostina, A., Zhelnin, M., Swaroop, S., Vedernikova, A., Bartolomei, M., Finite-element simulation of residual stresses induced by laser shock peening in TC4 samples structurally similar to a turbine blade, Frattura ed Integrità Strutturale, xx (2024) ww-zz.

Received: 30.09.2023
Accepted: 14.10.2023
Online first: xx.yy.zzzz
Published: xx.yy.zzzz

Copyright: © 2024 This is an open access article under the terms of the CC-BY 4.0, which permits unrestricted use, distribution, and reproduction in any medium, provided the original author and source are credited.

KEYWORDS. Laser shock peening, Numerical simulation, Titanium alloy, Residual stress.

INTRODUCTION

The important highly loaded components of modern aircrafts, such as turbine blades, require new techniques to extend their service life and prevent their expensive repair and replacement [1]. Among existing approaches, laser shock peening (LSP) technique have demonstrated remarkable efficiency in the aircraft and aerospace industries for improvement fatigue life of components and fatigue crack growth slowdown. The LSP technique allows performing

quick processing of metallic details and components with complex geometries and can be relatively easy incorporated in existing production lines [2].

During the LSP process, a metal surface under treatment is subjected to ultra-short high-energy laser pulses, which induce elastic-plastic waves into material [3]. As the Hugoniot elastic limit (HEL) of the material is exceeded, the propagation of the elastic-plastic waves produces the plastic strain. After the dynamic loading decays and static equilibrium of the detail is attained, the plastic strain leads to the occurrence of beneficial compressive residual stress in the subsurface layer. The compressive residual stress generated by LSP can reach high amplitude of about ~1 GPa and extend into material up to depth of several millimeters [4]. Besides, laser shots only slightly disturb surface roughness [5], but noticeably improve surface hardness [6, 7].

To study an influence of LSP on turbine blades numerical simulation is effectively used. Fang et al. [8] developed a 3D-model with of TC4 titanium alloy turbine blade in Ansys/LS Dyna software. Elastic-plastic behavior of the blade under laser impacts is described using the Johnson-Cook constitutive relation. To solve the governing equations of the model, an explicit algorithm based on the finite-element method was proposed. The one-sided and simultaneous two-sided LSP process was simulated for round laser spots applied to cross-sectional bands on the blade surface near its tip.

Li et al. [9] modified the model by making it two steps with the explicit dynamic analysis of shock waves propagation in the blade and the implicit static analysis of formation of the residual stress field. It was shown that an increase in the laser power density gains the compressive RSD inside the blade and its penetration depth.

Lin et al. [10] proposed 3D finite element model to describe an effect of a cuboidal projectile on a change in the RSD in airfoil previously subjected to LSP. The RSD induced in airfoil by laser shots was introduced into the model by solving linear elastic problem with additional strain, which were measured by synchrotron X-ray diffraction in the peened airfoil sample. The Johnson-Cook material and failure models were adopted to describe plastic deformation and dynamic failure of the airfoil on the projectile impact. Numerical analysis showed that LSP suppresses an occurrence of tensile stress in the notch of the airfoil after the impact.

Nie et al. [11] developed a model with dynamic explicit and static implicit steps in the Abaqus software to study reflection and coupling of the shock wave induced by laser shots in a thin TC17 titanium alloy blade profile. It was shown that the transverse plastic strain induced by the first compression wave gradually decreases due to the action of the subsequent reflected tensile wave and the residual tensile stress is formed. On the basis of the numerical results wave-transmitting layer to eliminate the shock wave reflection was proposed.

Xu et al. [12] proposed two steps model of the LSP process of the stainless steel turbine blade in the Abaqus software. To compute the compressive RSD, the Von Mises yield criterion with the HEL is employed. Numerical simulation was conducted for the treatment of the blade surface near the tenon end by laser spots of square shape. It was concluded that the increase in overlapping ratio enhances the uniformity and penetration depth of the compressive RSD.

Fameso et al. [13] developed in the Abaqus a model of laser shots impact on chromium based martensitic steel turbine blade used the explicit integral finite-element analysis employing time-dependent damping. The approach enables uniting both the shock wave propagation due to the dynamic loading and their time free damping to saturation points. Therefore, the overall LSP process with multiple impacts can be simulated in a single computation step. Another feature of the model is a use of the mechanical threshold stress constitutive relations, which allows replicating stepwise hardening of the material during the plastic deformation.

In the present paper, we investigate the effect of LSP on the generation of residual stress in a titanium super-alloy samples structurally similar to a turbine blade using a 3D finite-element model of the LSP process developed in [14]. This model incorporates a dynamic explicit step to compute an elastic-plastic waves propagation induced by a laser pulse and a static implicit step to determine RSD. Plastic deformation under laser impacts is described adopting the associated yield flow rule with the Johnson-Cook material model. The verification of the model was conducted based on the experimental measurements of RSD induced by LSP in square plates. The model was utilized to obtain distribution of residual stress under various peening regimes. On the basis of the numerical results the influence of the peening parameters is discussed.

NUMERICAL SIMULATION OF THE LASER SHOCK PEENING

According to [15-16] the LSP is considered as a purely mechanical process without simulation of ablation of material from the peened surface and generation of high temperature plasma. An effect of the laser pulse is simulated through a function of mechanical pressure applied to the peened surface. The shape, amplitude and time duration of pressure pulse was estimated based on one dimension plasma expansion model [17].

Numerical simulation of stress-strain state evolution of a sample subjected to the LSP process is conducted in the Simulia Abaqus software. An effect of each laser pulse is determined through two computational steps. The first step involves modeling of the propagation of the elasto-plastic waves in the material using the Explicit Solver due to the high amplitude and short duration of the pulse. In this step an irreversible strain induced by the impact loading is determined. The step ends as the plastic strain is stabilized. The duration of the step usually exceeds the duration of the pulse impact by two orders of magnitude [15].
The stress, strain, and displacement fields obtained during the dynamic explicit step are used as the initial conditions for the second step. At this step, a static equilibrium analysis is performed to determine the RSD. The component is not subjected external loading at this stage and the stress field is induced by the plastic strain that occurs in the dynamic step [16]. To conduct the static equilibrium analysis, the Implicit Solver is used that allows increasing the stability of the solving process. For the next laser shot, the results provided by the static analysis are transferred as initial conditions for the following dynamic step. In the case of the LSP with multi laser shots, the computational process is automated by programming the algorithm in Python.

Material model

From mechanical point of view, the LSP process is characterized by plastic deformation of the treated material with high strain rate, which exceeds 10^6 s^{-1}. The Johnson-Cook material model provides an adequate estimation of the plastic strain accounting for effects of strain hardening, strain rate and temperature softening.
As the temperature softening during the LSP could be neglected [16], the Johnson-Cook plasticity model can be written as:

$$F = \sigma_{eq} - \left[A + B\left(\varepsilon_{eq}^{pl}\right)^{n} \right] \left[1 + C \ln \frac{\dot{\varepsilon}_{eq}^{pl}}{\dot{\varepsilon}_0} \right] \tag{1}$$

where σ_{eq} is the equivalent stress, ε_{eq}^{pl} is the equivalent plastic strain, $\dot{\varepsilon}_{eq}^{pl}$ is the equivalent plastic strain rate, $\dot{\varepsilon}_0$ is a reference plastic strain rate, A, B, C, n are material parameters. The reference plastic strain rate $\dot{\varepsilon}_0$ is in the range of quasi-static tests. The parameter A corresponds to the initial value of the yield stress under quasi-static test. The parameters B, n describe strain hardening. The parameter C is responsible for the strain rate sensitivity.
For titanium alloy TC4 material constants and the Johnson-Cook material parameters are presented in Tab. 1. The elastic behavior of the alloy is described by Hooke's law for isotropic material, so only Young modulus and Poisson's ratio are provided.

Parameters	Values	Units	Symbol
Density	4424	kg/m^3	ϱ
Young's modulus	106.7	GPa	E
Poisson's ratio	0.314	-	ν
Quasi-static yield stress	978	MPa	A
Strengthening coefficient	826	MPa	B
Strain hardening exponent	0.639	-	n
Strain rate sensitivity parameter	0.034	-	C
Reference strain rate	0.005	1/s	$\dot{\varepsilon}_0$

Table 1: Material parameters for TC4.

Pressure equation

During the LSP process, the pressure pulse on the surface of the target is induced by the thermal expansion of the high-temperature plasma generated by the laser impact. However, following to [15, 16], the effects caused by the plasma generation can be neglected. In this case, the influence of the laser impact on the treated surface is described through the pressure boundary condition.

Because the laser spot is square, it can be assumed that the pressure generated by the laser impact is spatially uniformly distributed [12, 16]. To approximate the temporal variation of the pressure pulse, the triangular method is adopted for the LSP simulation [18]. According to the assumptions, the pressure function is written as:

$$P(t)=\begin{cases}\dfrac{t}{t_1}P_{peak}, & 0\le t<t_1\\ \dfrac{t_2-t}{t_1}P_{peak}, & t_1\le t\le t_2\end{cases} \tag{2}$$

where $t1 = 2\tau$ is the time of pressure increase, $t2 = 8\tau$ is the time of pressure decrease, $\tau = 10$ ns is the laser pulse duration, $Ppeak$ is the peak pressure value. Parameters $t1$ and $t2$ for TC4 alloy were determined in our previous work [14] and verified for a large range of laser peak intensities from 3.3 GW/cm² to 40 GW/cm². The total simulation time is equal to 10 μs that ensures stabilization of the plastic strain in the target.

To estimate the peak pressure, the one dimension Fabro model of ablation is adopted [19]:

$$P_{peak}=0.01\sqrt{\frac{\alpha}{2\alpha+3}\cdot Z\cdot I} \tag{3}$$

where $Z = (2\cdot Z_{water}\cdot Z_t) / (Z_{water}+Z_t)$ is the combined acoustic impedance of water ($Z_{water} = 0.17\cdot 10^6$ g/(cm²·s)) and target ($Z_t = 1.7\cdot 10^6$ g/(cm²·s) for aluminum foil [19]), α is the efficiency coefficient which is typically equal to 0.33, I is the maximum energy density (10 GW/cm² in our case).

MODEL VERIFICATION

In order to verify the FE simulation result, the LSP experiment was performed for some specimens from TC4 titanium alloy. Fig. 1 shows geometry of the specimen (covered with aluminum foil) and the model specimen. The plate's thickness is 2 mm. The measurement of the residual stresses values versus the depth of the treated layer was carried out by the hole drilling method using an automatic system MTS3000-Restan (according to ASTM E837-13a [20]). This method has a number disadvantages such as flat surface of the specimen, measurements only in one point of the surface, selection of suitable strain gauge sizes if specimen is small enough, providing only two components of residual stress and etc. The averaging area for RSD in FEM corresponded to the drill size in the experiment.

Comparison was conducted for two LSP cases:

1. square spots of 1 mm and power density of 10 GW/cm² (which is equal to 5.3 GPa) without overlapping;
2. double pass with square spots of 1 mm and power density of 10 GW/cm².

The numerical distribution of the residual stresses at the surface of the specimen for case 1 and case 2 is shown in Fig. 2. In depth distribution of residual stresses for LSP cases 1 and 2 are shown in Fig. 3. Residual stress components σ_x and σ_y show close values at all depths. This indicates the isotropy of created residual stress on the surface. The maximum value of both compressive residual stress components is on the specimen surface and equal to 240 MPa approximately after the first pass (case 1) and to 380 MPa approximately after the second pass (case 2). The depth of the compressive residual stress field according to the graph in Fig. 3 is about 0.6 mm.

The difference in minimum value of residual stress between experimental and numerical results is nearly 10%. This minor disagreement can be explained by possible measurement inaccuracies of the incremental hole drilling method due to its incremental and destructive character.

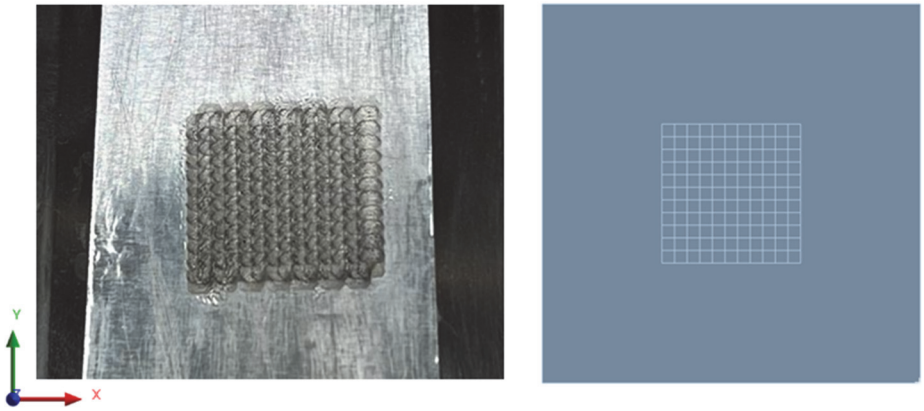

(a) (b)

Figure 1: Treated surface: (a) the sample covered with foil, (b) the FE model.

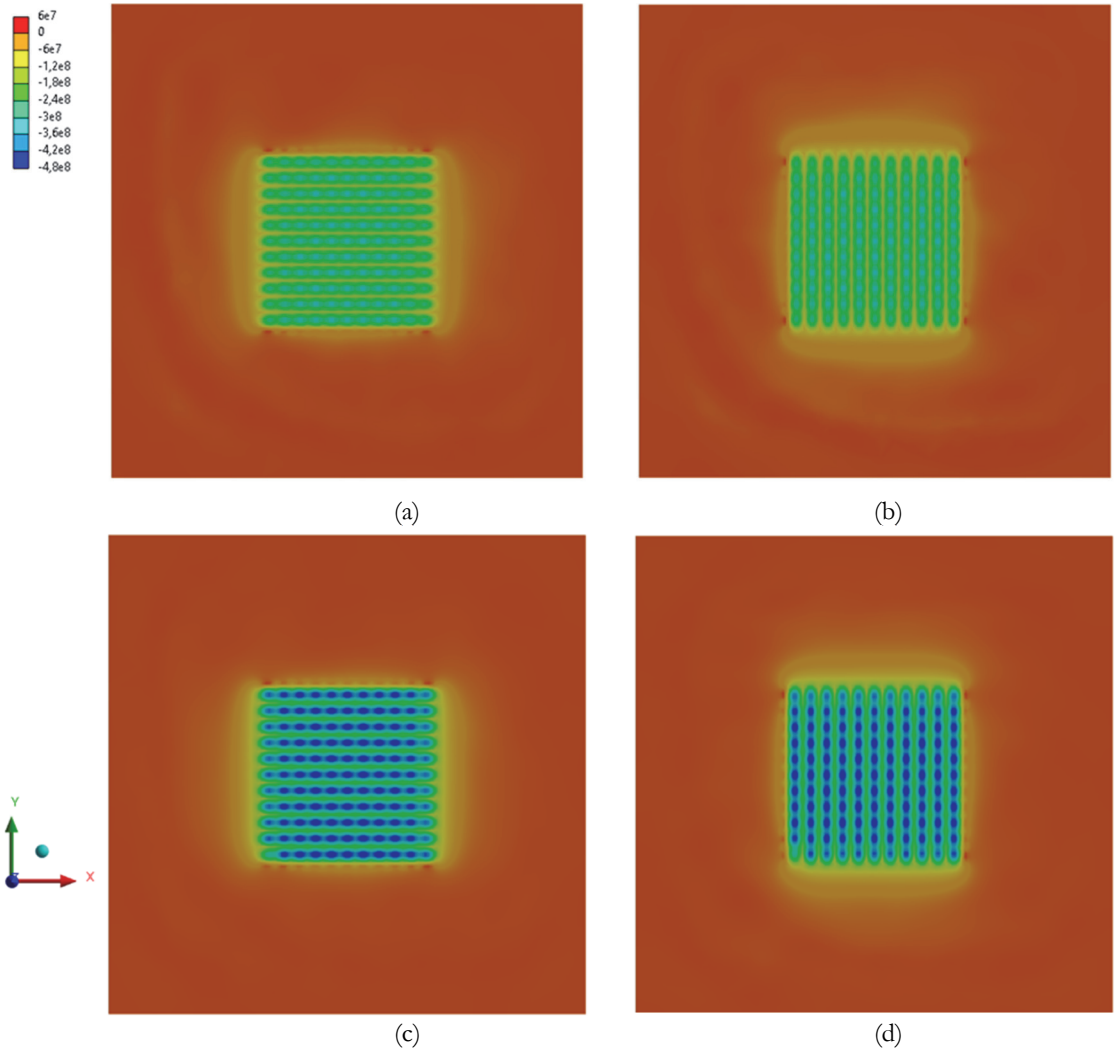

(a) (b)

(c) (d)

Figure 2: Residual stress after LSP: (a) σ_x for case 1, (b) σ_y for case 1, (c) σ_x for case 2, (d) σ_y for case 2.

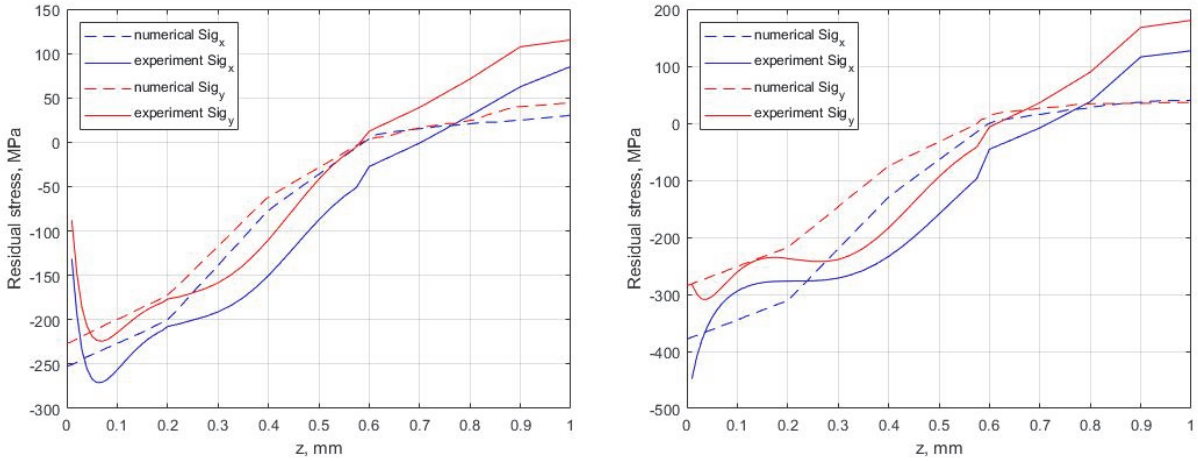

Figure 3: Residual stress comparison: (a) case 1, (b) case 2.

RESULTS AND DISCUSSION

The above-explained model was applied to predict RSD induced by LSP of edges of samples structurally similar to a turbine.

The sample was discretized by eight-node brick elements with reduced integration and hourglass control (C3D8R) in the LSP region. To obtain precise results, a high-density mesh (0.1mm x 0.1mm x 0.05 mm) was utilized in the LSPed zone. The example of finite element discretization is shown in Fig. 4. The root of the sample was assumed to be fixed. This condition represent the robotic arm's grip on the specimen during the LSP process. LSP was performed with square spots. The size of the spot, the laser energy and overlapping of the spots were varied to investigate the effect of LSP parameters.

Fig. 5 shows typical distribution of the mechanical pressure for two-sided peening of the sample edges. This figure provides information on mean stresses of the three diagonal stress tensor components. It can be seen that compressive RSD are formed for lower and upper sides (corresponding to concave and convex sides) of the sample. Due to an intricate shape of the sample the distribution is non-uniform. The maximum value of compressive mean stress is around 400 MPa and it is located on the surface of the sample while the maximum tensile pressure is inside the volume of the part.

Fig. 6 depicts characteristic distribution of effective plastic strain. LSP induces initiation of inelastic strains in the peening region. The average magnitude of effective plastic strain is around 4%. In comparison with mechanical pressure, the effective plastic strain is distributed more uniformly.

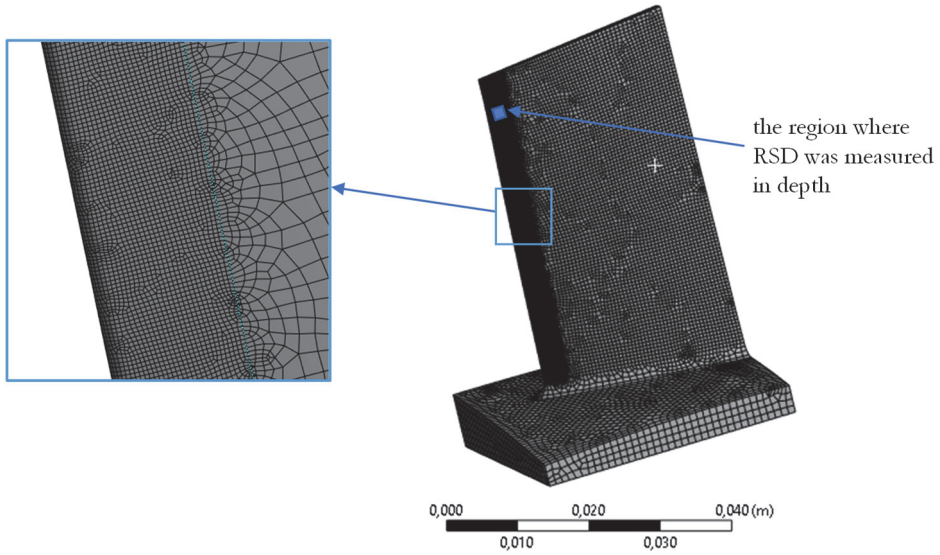

Figure 4: The example of mesh discretization.

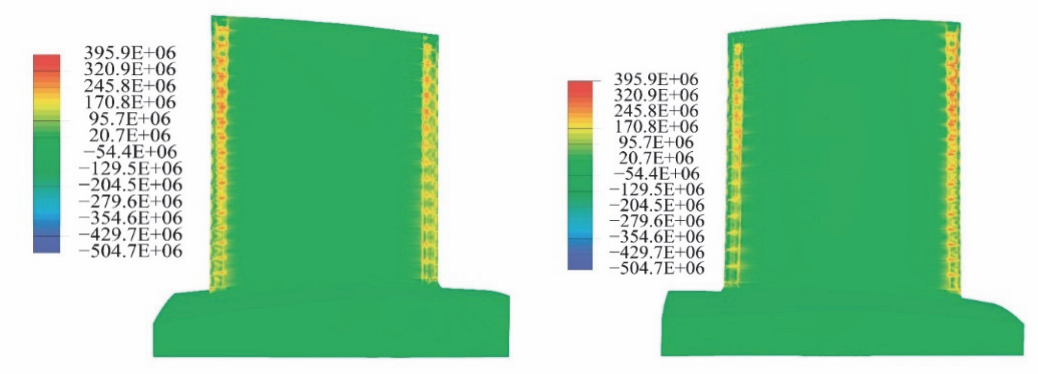

(a) (b)

Figure 5: Characteristic distribution of mechanical pressure: (a) lower side of the sample, (b) upper side of the sample.

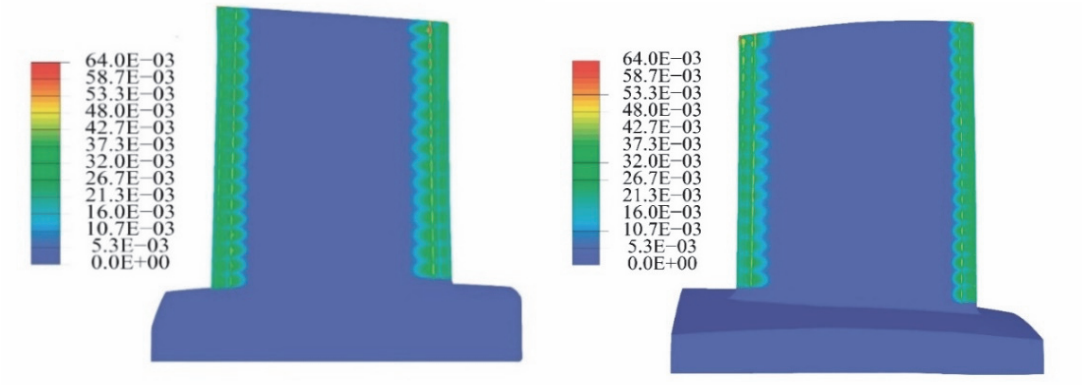

(a) (b)

Figure 6: Characteristic distribution of effective plastic strain: (a) lower side of the sample, (b) upper side of the sample.

Since RSD is non-uniform, we investigate the effect of LSP parameters on the upper part of the blade, which is more frequently subjected to damage during service according to the aircraft statistics. The area of interest is a rectangular parallelepiped, whose height is equal to the height of the sample and the base is a square with a size of 1 mm. The center of this area is located at the distance of 4.5 mm from the upper boundary of the sample and at the distance 1 mm from the edge of the sample (Fig. 4). We consider LSP with two different spot sizes: 1 mm and 3 mm. The energy intensity and overlapping of the spots are varying parameter during the numerical analysis. Therefore, we investigate the effect of spot size, laser energy and overlapping of the laser spots on in-depth RSD. The maximum stress tensor component is averaged over the area of interest to obtain the resulting RSD.

Fig. 7 presents results for LSP of the sample with square spots of 3 mm without overlapping and two different laser intensities of 1.11 GW/cm^2 and 10 GW/cm^2. According to Eqn. (3), these power densities correspond to the 1.76 GPa and 5.3 GPa respectively.

From Fig. 7(a) it can be seen that no compressive residual stresses are obtained on the surfaces of the sample. The compressive stress is concentrated from 0.15 mm to 0.52 mm from the upper surface. This can be explained by the high value of the yield stress for TC4 (Tab. 1) and low value of loading. In comparison with this result, the in-depth RSD shown in Fig. 7(b) demonstrates that all stresses are compressive. The value on the front surface is equal to -250 MPa, the value on the opposite surface is slightly higher and equal to -300 MPa. When approaching to the center of the sample, the magnitude of residual stress reduces. The minimum value of compressive RSD is in the middle of the thickness and is equal to 50 MPa. The distribution is asymmetrical since the sample has the varying thickness. The presented results show that increase in the power density induces rise in the magnitude of compressive residual stress. Too humble values of laser intensities cannot produce compressive residual stress on the surface of the treated object.

Fig. 8 shows effect of overlapping on the in depth RSD for the small power density equal to 1.1 GW/cm^2.

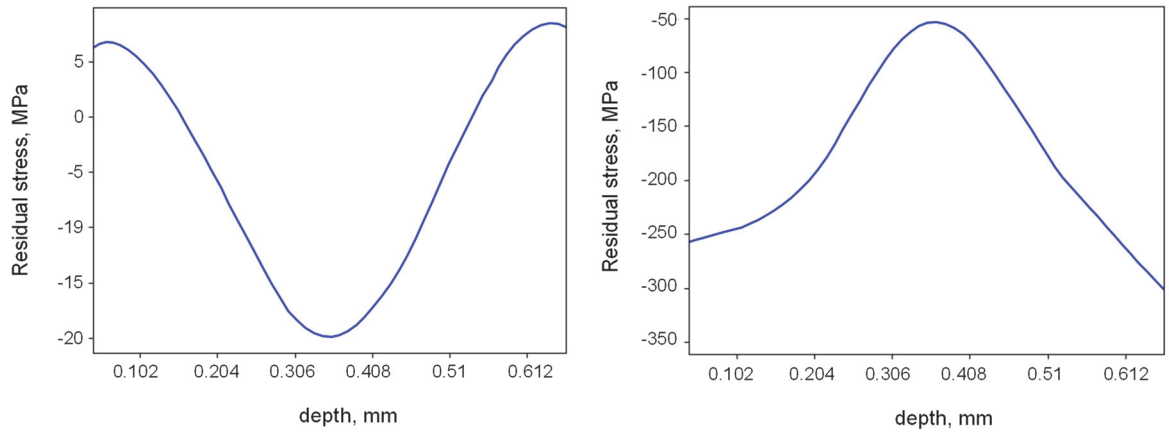

(a) (b)

Figure 7: Residual stress for square spot of 3 mm without overlapping (a), P = 1.76 GPa (I = 1.11 GW/cm^2), (b) P=5.3 GPa (I = 10 GW/cm^2).

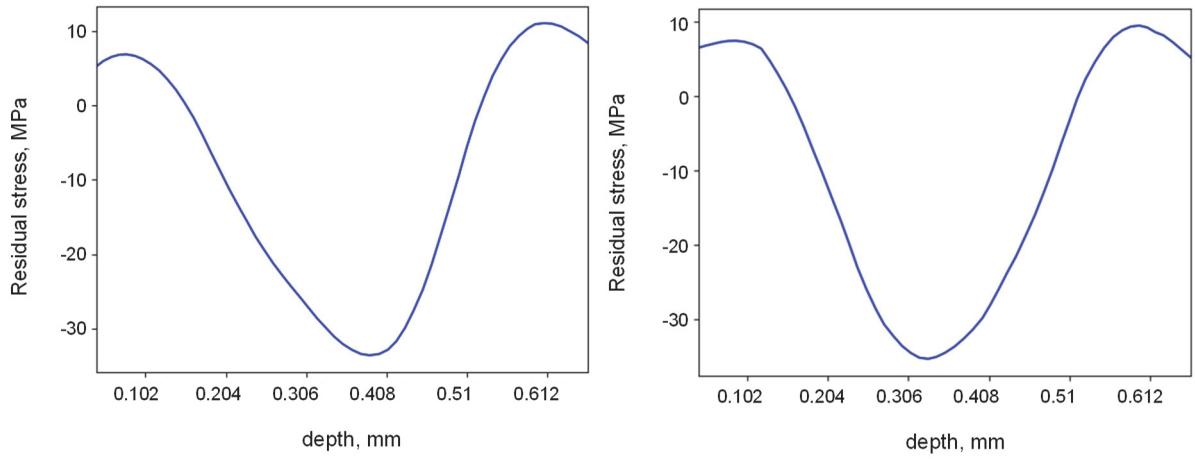

(a) (b)

Figure 8: Residual stress for square spots of 3 mm (a) with 35% overlapping and P = 1.76 GPa (I = 1.1 GW/cm^2), (b) 50% overlapping and P = 1.76 GPa (I = 1.1 GW/cm^2).

Comparison with Fig. 7(a) shows that overlapping cannot enhance value of residual stress on the surface. For both overlappings of 35% and 50% the residual stresses at the surface are tensile similar to Fig. 7(a). However, it can be seen that there is slight decline in the residual stress value in the middle of the thickness with the increase in overlapping rate. But still the profiles are qualitatively similar. Therefore, it can be concluded that increase in overlapping for a humble power density cannot improve the in-depth RSD. The power density has larger effect than overlapping of the laser spots.

Fig. 9 presents results obtained for LSP with square spots of 1 mm and power density of 10 GW/cm^2 (which is equal to 5.3 GPa) with overlapping of 0% and 35%.

Comparison with Fig. 7(b) shows that application of smaller spots increases magnitude of compressive residual stress in the area of interest. Similar to Fig. 7(b) the profile shows compressive state. However, the value on the front surface in Fig. 8(a) is -300 MPa and on the opposite surface is around 350 MPa. Hence, this treatment regime enhances residual stress on 20% in the area of interest compared with the Fig. 7(b). Also, LSP with smaller spots induces two peaks in in-depth profile. The uniform RSD when applying spots of larger size [21] can attribute this. Overlapping 35% presented in Fig. 9(b) improves residual stress. The value at the front surface becomes -425 MPa. On the opposite surface it reaches almost - 625 MPa. The minimum value is at the middle of the thickness and is equal to 350 MPa.

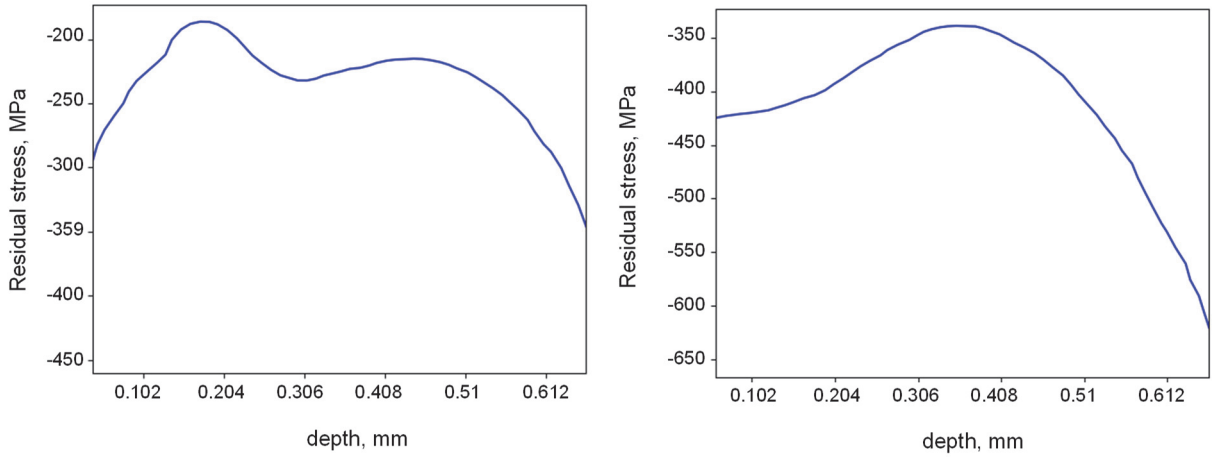

Figure 9: Residual stress for square spots of 1 mm (a) without overlapping and P = 5.3 GPa (I = 10 GW/cm²), (b) with 35% overlapping and P = 5.3 GPa (I = 10 GW/cm²).

Thus, it can be concluded that LSP regime with overlapping increases non-uniformity in in-depth distribution of residual stress. At the same time, the surface and, as a consequence, subsurface RSD becomes more homogenous and two peaks vanish. The qualitative distribution shifts to the case of LSP with larger spots similar to the presented in Fig. 7(b).

Conclusions

The objective of this study to investigate RSD in TC4 samples structurally similar to a turbine blade induced by LSP with varying parameters using finite-element analysis. A mathematical model is based on the strain rate sensitive Johnson-Cook constitutive equation. The model considers LSP as a purely mechanical process, where all effects related to the plasma influence on the treated surface are taken into account by a spatially uniform time-varying pressure pulse. A two-step approach was used in the applied LSP model, where dynamic and static problems were solved successively to obtain the RSD after each shot.

In order to investigate the impact of peening parameters on residual stresses, a series of numerical calculations were conducted. The edges of the samples were peened with square spots at the upper and lower sides simultaneously. Two sizes of square spots were considered (1 mm and 3 mm). The laser energy and overlapping of the spots were varied. The analyzed in depth RSD were located at the most vulnerable part of the sample. Based on the obtained results, the following main conclusions can be drawn.

- An increase in the power density results in a rise in the magnitude of compressive residual stress. Laser intensity equal to 1.11 GW/cm² cannot produce compressive residual stress on the surface of the treated object because of the high value of TC4 yield stress. Laser intensity equal to 10 GW/cm² induces compressive residual stress of 250 MPa on the upper side of the sample and -300 MPa on opposite side of the sample.
- Increase in overlapping of the spots for a low power density (1.11 GW/cm²) cannot induce compressive residual stress on the treated surface.
- Decrease in spot size from 3 mm to 1 mm allows increasing of magnitude of compressive residual stress on 20% in the area of interest. Applying 35% overlapping enhances this value even more. Moreover, the surface and subsurface RSD becomes more homogeneous.

Acknowledgments

The reported study was supported by the Government of Perm Krai, research project No. C-26/829. LSP treatment was carried out under financial support from the Programs for the creation and development of the world-class scientific center "Supersound" for 2020–2025 with the financial support of the Ministry of Education and Science of Russia (Agreement No. 075-15-2022-329 dated April 21, 2022).

REFERENCES

[1] Zhang, X., Yang, M., Zhou, C., Fu, N., Huang, W. and Wang, Z. (2022). A comprehensive review of fatigue behavior of laser shock peened metallic materials, Theoretical and Applied Fracture Mechanics, 122, 103642. DOI: 10.1016/j.tafmec.2022.103642.

[2] Zhang, C., Dong, Y. and Ye, C. (2021). Recent developments and novel applications of laser shock peening: A review, Advanced Engineering Materials, 23(7), 2001216. DOI: 10.1002/adem.202001216.

[3] Peyre, P., Fabbro, R., Berthe, L. and Dubouchet, C. (1996). Laser shock processing of materials, physical processes involved and examples of applications, Journal of Laser Applications, 8(3), pp. 135-141. DOI: 10.2351/1.4745414.

[4] Hu, J. L., Lou, J., Sheng, H. C., Wu, S. H., Chen, G. X., Huang, K. F. and Yin, S. (2012). The effects of laser shock peening on microstructure and properties of metals and alloys: a review, Advanced Materials Research, 347, pp. 1596-1604. DOI: 10.4028/www.scientific.net/AMR.347-353.1596.

[5] Gao, Y. K. (2011). Improvement of fatigue property in 7050–T7451 aluminum alloy by laser peening and shot peening, Materials Science and Engineering: A, 528(10-11), pp. 3823-3828. DOI: 10.1016/j.msea.2011.01.077.

[6] Ebrahimi, M., Amini, S. and Mahdavi, S. M. (2017). The investigation of laser shock peening effects on corrosion and hardness properties of ANSI 316L stainless steel, The International Journal of Advanced Manufacturing Technology, 88, pp. 1557-1565. DOI: 10.1007/s00170-016-8873-0.

[7] Zhang, J., Cheng, X., Xia, Q. and Yan, C. (2020). Strengthening effect of laser shock peening on 7075-T6 aviation aluminum alloy, Advances in Mechanical Engineering, 12(8), 1687814020952177. DOI: 10.1177/1687814020952177.

[8] Fang, Y. W., Li, Y. H., He, W. F. and Li, P. Y. (2013). Effects of laser shock processing with different parameters and ways on residual stresses fields of a TC4 alloy blade, Materials Science and Engineering: A, 559, pp. 683-692. DOI: 10.1016/j.msea.2012.09.009.

[9] Li, P., Huang, S., Xu, H., Li, Y., Hou, X., Wang, Q. and Fang, Y. (2015). Numerical simulation and experiments of titanium alloy engine blades based on laser shock processing, Aerospace Science and Technology, 40, pp. 164-170. DOI: 10.1016/j.ast.2014.10.017.

[10] Lin, B., Zabeen, S., Tong, J., Preuss, M. and Withers, P. J. (2015). Residual stresses due to foreign object damage in laser-shock peened aerofoils: Simulation and measurement, Mechanics of Materials, 82, pp. 78-90. DOI: 10.1016/j.mechmat.2014.12.001.

[11] Nie, X., Tang, Y., Zhao, F., Yan, L., Wu, H., Wei, C. and He, W. (2021). Formation mechanism and control method of residual stress profile by laser shock peening in thin titanium alloy component, Materials, 14(8), 1878. DOI: 10.3390/ma14081878.

[12] Xu, G., Luo, K. Y., Dai, F. Z. and Lu, J. Z. (2019). Effects of scanning path and overlapping rate on residual stress of 316L stainless steel blade subjected to massive laser shock peening treatment with square spots, Applied Surface Science, 481, pp. 1053-1063. DOI: 10.1016/j.apsusc.2019.03.093.

[13] Fameso, F. (2020). Explicit analysis using time-dependent damping simulation of one-sided laser shock peening on martensitic steel turbine blades, Simulation: Transactions of the Society for Modeling and Simulation International, 96(12), pp. 927–938. DOI: 10.1177/0037549720954272.

[14] Kostina, A., Zhelnin, M., Gachegova, E., Prokhorov, A., Vshivkov, A., Plekhov, O. and Swaroop, S. (2022). Finite-element study of residual stress distribution in Ti-6Al-4V alloy treated by laser shock peening with varying parameters, Frattura ed Integrità Strutturale, 16(61), pp. 419–436. DOI: 10.3221/IGF-ESIS.61.28.

[15] Braisted, W. and Brockman, R. (1999). Finite element simulation of laser shock peening, International Journal of Fatigue, 21, pp. 719-724. DOI: 10.1016/S0142-1123(99)00035-3.

[16] Keller, S., Chupakhin, S., Staron, P., Maawad, E., Kashaev, N. and Klusemann, B. (2018). Experimental and numerical investigation of residual stresses in laser shock peened AA2198, J. Mater. Process. Technol., 255, pp. 294-307. DOI: 10.1016/j.jmatprotec.2017.11.023.

[17] Fabbro, R., Fournier, J., Ballard, P., Devaux, D. and Virmont, J. (1990). Physical study of laser-produced plasma in confined geometry, J. Appl. Phys., 68, pp. 775-784. DOI: 10.1063/1.346783.

[18] Wang, C., Li, K., Hu, X., Yang, H. and Zhou, Y. (2021). Numerical study on laser shock peening of TC4 titanium alloy based on the plate and blade model, Optics & Laser Technology, 142, 107163. DOI: 10.1016/j.optlastec.2021.107163.

[19] Langer, K., Spradlin, T. J. and Fitzpatrick, M. E. (2020). Finite element analysis of laser peening of thin aluminum structures, Metals, 10, 93. DOI: 10.3390/met10010093.

[20] Rendler, N.J. and Vigness, I. (1966). Hole-drilling strain-gage method of measuring residual stresses, Experimental Mechanics, 6, pp.577–586. DOI: 10.1007/BF02326825.

[21] Sun, R., Li, L., Zhu, Y., Zhang, L., Guo, W., Peng, P., Li, B., Guo, C., Liu, L. and Che, Z. (2017). Dynamic response and residual stress fields of Ti6Al4V alloy under shock wave induced by laser shock peening, Modelling and Simulation in Materials Science and Engineering, 25(6), 065016. DOI: 10.1088/1361-651X/aa7a46.